

Microstructure and Crystallographic Texture Evolution During the Friction-Stir Processing of a Precipitation-Hardenable Aluminum Alloy

NARESH NADAMMAL,¹ SATISH V. KAILAS,¹ JERZY SZPUNAR,² and SATYAM SUWAS^{3,4}

1.—Department of Mechanical Engineering, Indian Institute of Science, Bangalore, India.
2.—Department of Mechanical Engineering, University of Saskatchewan, Saskatoon, Canada.
3.—Department of Materials Engineering, Indian Institute of Science, Bangalore, India.
4.—e-mail: satyamsuwas@materials.iisc.ernet.in

Friction-stir processing (FSP) has been proven as a successful method for the grain refinement of high-strength aluminum alloys. The most important attributes of this process are the fine-grain microstructure and characteristic texture, which impart suitable properties in the as-processed material. In the current work, FSP of the precipitation-hardenable aluminum alloy 2219 has been carried out and the consequent evolution of microstructure and texture has been studied. The as-processed materials were characterized using electron back-scattered diffraction, x-ray diffraction, and electron probe microanalysis. Onion-ring formation was observed in the nugget zone, which has been found to be related to the precipitation response and crystallographic texture of the alloy. Texture development in the alloy has been attributed to the combined effect of shear deformation and dynamic recrystallization. The texture was found heterogeneous even within the nugget zone. A microtexture analysis revealed the dominance of shear texture components, with C component at the top of nugget zone and the B and A₂* components in the middle and bottom. The bulk texture measurement in the nugget zone revealed a dominant C component. The development of a weaker texture along with the presence of some large particles in the nugget zone indicates particle-stimulated nucleation as the dominant nucleation mechanism during FSP. Grain growth follows the Burke and Turnbull mechanism and geometrical coalescence.

INTRODUCTION

Aluminum with copper as a major alloying element (2XXX series) is the most common age-hardenable alloy system that has been studied extensively, and these alloys are widely used in critical structural applications.¹ Some alloys of this series also contain magnesium, which imparts the required damage-tolerance property. The precipitates in this alloy system are Al₂Cu and Al₂CuMg, which lead to strengthening. An additional degree of strengthening can be imparted by grain refinement. Severe plastic deformation (SPD) techniques, like equal-channel angular pressing, high-pressure torsion, accumulative roll bonding, multiaxial forging, and friction-stir processing^{2–8}

offer ample scope for grain refinement in aluminum alloys. In addition, these processes lead to characteristic crystallographic texture development, which is also important for the performance of the processed materials.^{9,10}

Friction-stir processing (FSP)¹¹ has been perceived as a process leading to grain refinement and also as a surface-modification technique. In FSP, a nonconsumable rotating tool with a shoulder and a pin is traversed along the specific region on a material, which is to be subjected to grain refinement. The most significant advantage of FSP compared with any other SPD technique^{12,13} is that the tooling is much simpler and the process is less energy intensive. Furthermore, there is no limitation of size and shape for the work piece.

Table I. Elemental composition of the alloy AA 2219

<u>Element</u>	<u>Al</u>	<u>Cu</u>	<u>Mn</u>	<u>Si</u>	<u>Zr</u>	<u>V</u>	<u>Ti</u>	<u>Zn</u>
wt.%	94.23	5.2	0.17	0.15	0.1	0.1	0.03	0.02

Though not much information is available from the existing FSP literature, the micro and bulk crystallographic texture development and their correlation in the processed materials¹⁴ are as much important as the microstructure evolution. As the tool pin rotates and stirs a fixed volume of material continuously at high rotation speeds during FSP, it is possible that there can be local variations in texture within the nugget zone. This variation can also happen due to the different amounts of strain and temperature experienced by different regions of the nugget zone. Hence, it is also important to study the microtexture at various points in the nugget zone.

In view of the preceding discussion, the objective of the current work is to focus on the important aspects of microstructure evolution and crystallographic texture development during the single-pass and multipass FSP samples. The alloy AA 2219 has been chosen particularly due to its obvious industrial significance.¹⁵ This alloy has been processed using an optimum set of parameters, and the consequent evolution of texture and microstructure has been done using x-ray diffraction and scanning electron microscopy-based techniques.

EXPERIMENTAL

The material selected for the current study is the aluminum alloy 2219 of 7.2 mm in thickness, which is a heat-treatable alloy with copper as the major alloying element. The material was received in the T87 temper, which is a solution that was heat treated and cold worked approximately 7–10% and then artificially aged. The elemental composition of the as-received alloy was determined using a JEOL JXA-8530F (JEOL Ltd., Tokyo, Japan) electron probe microanalyzer (EPMA) and is given in Table I.

The tool was made of hot die steel (HDS) in H13 hardened condition. The tool shoulder diameter was of 26 mm tapered from a 28 mm cylinder, with tool pin shaped as that of a frustum of a cone with a top diameter of 6 mm and a bottom diameter of 4 mm. A tool pin length of 5.4 mm with a righthand thread having a pitch of 1.5 mm was used for the plate thickness of 7.2 mm. The threaded tool geometry selection was made because such a feature will allow better material mixing during processing, especially due the vertical movement of the material.

The process parameters of FSP were optimized using a method developed by the authors in Ref. 16

Based on this approach, the optimized parameters for this alloy were a tool rotation speed of 650 RPM, a tool traverse speed of 125 mm/min, and a tool plunge depth of 0.25 mm into the work piece.

The optimum single pass processed samples were subjected to detailed microstructural characterization. The transverse cross sections of the samples were metallographically polished. The polished samples were etched using Keller's reagent (95 mL distilled water, 2.5 mL HNO₃, 1.5 mL HCl, and 1 mL HF) for characterization using optical microscopy (OM). A macroimage of the processed zone was captured using a low-magnification optical microscope that allows a total magnification from 7 times to 50 times. OM for microstructural analysis was done on a Metallovert Carl Zeiss microscope (Carl Zeiss, Oberkochen, Germany) having an eyepiece lens of 10 times magnification.

For characterization using electron microscopy, the final polished samples were electro polished using Struers Lectropol-5 electropolisher (Struers A/S, Ballerup, Denmark) with the standard A2 electrolyte. The electrolyte was kept in the refrigerator at a temperature of -5°C to 2°C , 1 h prior to polishing, and the parameters used were a voltage of 26 V and a time period of 20 s. Scanning electron microscopy (SEM) was done on an ESEM Quanta microscope (Quanta 200; FEI Company, Hillsboro, OR) and electron back-scattered diffraction (EBSD) facility available in the same SEM was used for the detailed microstructure and microtexture analysis. For EBSD analysis, all the specimens were kept in SEM in a similar way so that while analyzing the data, similar kinds of rotations can be made to match the frame of reference for shear deformation. These rotations were made in accordance with Ref. 17 EBSD scans were analyzed using TSL Orientation Imaging Microscopy (OIM) package (EDAX Inc., Mahwah, NJ). The standard cleaning up procedure was employed for removing the unindexed grain boundaries during the microstructure analysis. For the texture analysis of EBSD data, scan points with a confidence index (CI) of less than 0.1 were omitted from the consideration.

Bulk texture in the transverse cross section of the processed samples was measured on a Bruker D8 discover x-ray goniometer with an area detector (Vantec-500; Bruker AXS Inc., Madison, WI). General area detector diffraction system (GADDS) allows faster data collection in a shorter time compared to one-dimensional detectors.

RESULTS AND DISCUSSION

Microstructure Evolution in the Nugget Zone

Microstructure evolution during FSP of aluminum alloys is still not clear due to the complex thermomechanical mechanisms involved. It has been commonly observed in the FSP literature that a random set of parameters was used for processing. The most important aspect in FSW/FSP is the selection of optimum processed parameters that could give rise to a defect-free material. Hence, in the current work, we have optimized the process parameters based on a bottom-up approach and the same is detailed in Ref. 16 for a similar aluminum alloy 2024. The optimally processed samples have been characterized in detail.

Transverse cross section of the optimum parameter processed sample is shown in Fig. 1. Figure 1a displays various zones in the FSP sample at a lower magnification, whereas Fig. 1b shows the same at a higher magnification, which reveals the typical onion-ring structure found in some of the friction-stir processed aluminum alloys.

The micrograph reveals a preferential etching at the advancing side compared with the retreating side, which is represented by a sharp boundary in the advancing side. This occurs because of the larger gradients of strain and temperature in the advancing side.¹⁸ A diffused boundary is observed at the retreating side.

The detailed features in the onion ring were characterized using EBSD, and a scan taken in this region is shown in Fig. 2a and b. The inverse pole figure (IPF) map indicates a periodicity between the ring patterns (Fig. 2a) and the same is highlighted with black dotted lines. However, an image quality map (Fig. 2b) with grain boundaries superimposed on it shows no such periodicity and a rather uniform microstructure is observed throughout the region. For grain boundary characterization, boundaries

having misorientations of 3° – 5° and 5° – 15° are considered as very low-angle boundaries (VLABs) and low-angle boundaries (LABs), respectively, as they will depict the recovery processes occurring during FSP. Boundaries having misorientation higher than 15° are considered as high-angle grain boundaries. The average grain size observed in the onion-ring structure is the same as that observed for the other regions in the nugget zone.

Onion-ring formation in some materials is typical of the aftereffects of material flow during FSP, which is considered as a combination of an extrusion and forging process.¹⁸ The material extruded by the tool pin is forged by the tool shoulder and a new interface is created during FSP.¹⁹ The effect of this can also be observed in the transverse cross section when the ratio of tool rotation to translation is maintained. A detailed explanation for the formation of onion ring is reported elsewhere;²⁰ the focus in the current work is to present and analyze the microstructural features of the onion ring. Low-angle boundaries are observed in abundance at the grains in the onion ring, which shows that the deformation continues after DRX and a stable orientation has not yet reached. Shear texture components are observed with the dominance of C component in the band with random textures in the neighborhood on both sides. The Taylor factor is the highest for C component amongst all the shear texture components²¹ for face-centered cubic (fcc) materials and hence it is a relatively harder orientation.

Such a banded onion-ring structure has been reported by Sutton et al.²² in which the authors have attributed the banded structure as alternative particle-rich and particle-deficit regions. These particles can lead to particle-stimulated nucleation (PSN), which could be the dominant micromechanism in these regions leading to a weak texture.²³ In the particle-deficit regions, crystallographic texture can develop with the C component, in which shear plane

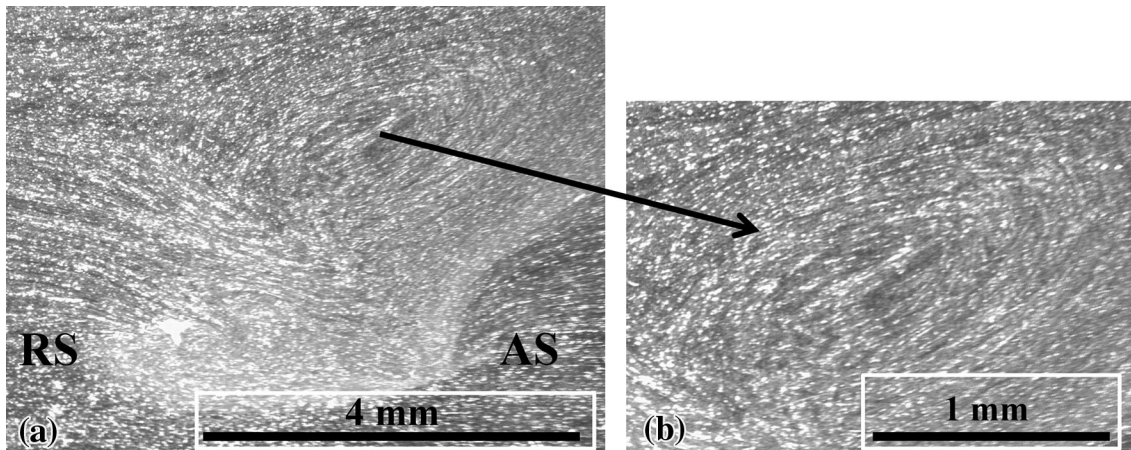


Fig. 1. Transverse cross section of the optimum processed sample: (a) processed zone with advancing side (AS) and retreating side (RS) marked (b) onion-ring pattern is highlighted.

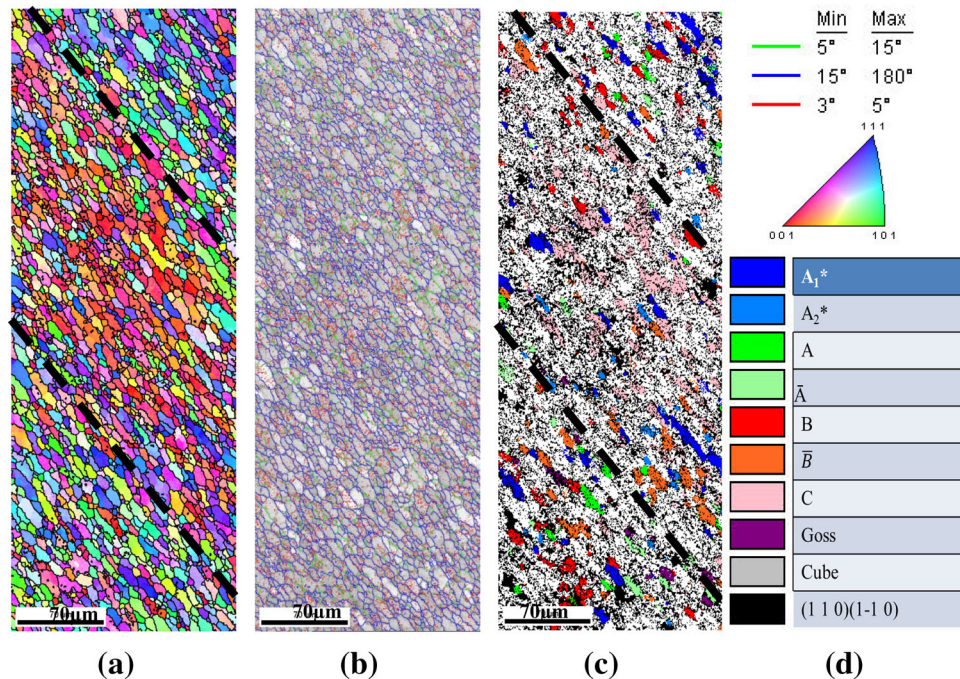


Fig. 2. EBSD maps corresponding to the onion ring feature: (a) IPF map, (b) IQ map, (c) texture map, and (d) color codes used for grain boundaries (top) and orientation (bottom).

normal is parallel to $\{001\}$ plane and the shear direction as $\langle 110 \rangle$. The formation of such a component is easier when the deformation mode is shear taking place at a higher temperature. Hence the development of a strong C component of texture in the alternative bands indicates that onion-ring formation is a texture-dependent phenomenon.

The microstructural observations of the nugget zone at different regions obtained from EBSD are shown in Fig. 3. These scans were taken at the exact center line of the nugget zone, 200 μm from the top, 1 mm from the top, in the middle and at 1.5 mm from the bottom of the nugget zone. Fine equiaxed and strain-free grains with an average grain size $\sim 4 \mu\text{m}$ are observed at the bottom of the nugget zone. Comparatively larger grains with high intragrain misorientations are observed at the top and middle of the nugget zone. The higher misorientations could be due to the continued deformation after recrystallization.²⁴

The misorientation profile for such a large grain is shown in Fig. 4. The IPF map shows this as a single grain because of the small deviation in orientation from the neighborhood, whereas the image quality (IQ) map, which is an indication of the quality of diffraction pattern observed shows the same as a large grain subdivided into subgrains.

Micromechanisms responsible for the microstructural evolution during FSP can be elucidated from the fine analyses of the EBSD scans. In FSP, deformation and annealing (due to the heat generated during processing) is a continuous process, and this will retain various stages of microstructural evolution in some of the grains that

do not acquire a stable orientation at once. Hence, a detailed analysis of the microstructural features can give sufficient information about the microstructural evolution during FSP. At temperatures as high as 400°C to 550°C and due to the highly tortuous deformation path followed by the material during FSP, dynamic recrystallization is one of most tentative mechanisms.²⁵ Possible nucleation and grain growth stages of dynamic recrystallization can be evaluated from the EBSD and SEM images in Fig. 5. In Fig. 5a, bulges are observed next to the grain boundary (indicated by a low-angle boundary). Such a region is depicted by 1 and the bulge boundaries are indicated by an arrow. This gives an idea about the nucleation stage of recrystallization. The precipitates (Fig. 5e) could increase the propensity of nucleation through the PSN mechanism. Elemental composition of the particle is given in Fig. 5f, and this corresponds to the equilibrium precipitate Al_2Cu found in the alloy 2219. Smaller particles are also observed in the micrograph, and it is possible that nucleation can occur more easily.

Continuous straining and temperature rise during FSP is likely to transform the low-angle boundaries (3° – 5°) to medium-angle boundaries (5° – 15°), as depicted by 2 in Fig. 5a. Similar features are apparent in Fig. 5b with the boundary surrounded partially by low- and medium-angle boundaries. A fully developed microstructure with high-angle boundaries, represented by stage 3, can be observed in Fig. 5a. With time, such high temperatures lead to the occurrence of thermodynamically favored processes, which eventually cause the formation of grain boundary triple

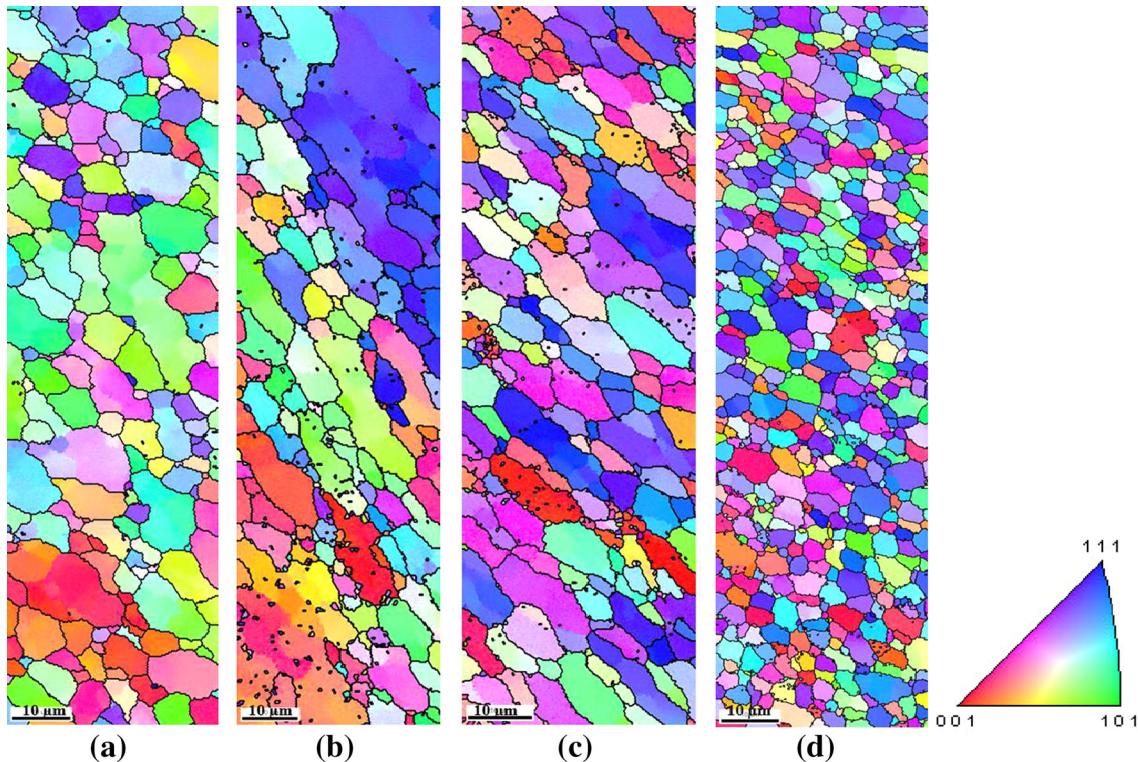


Fig. 3. IPF for EBSD scans taken across the thickness at the nugget zone: (a) 0.2 micron from the top of nugget zone, (b) 1 mm from top, (c) middle, and (d) 1.5 mm from the bottom.

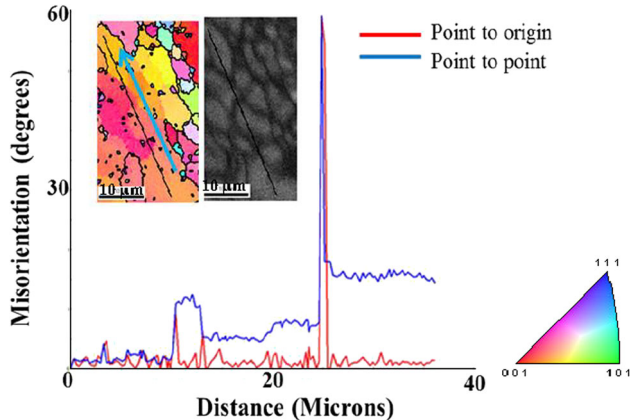


Fig. 4. Misorientation profile for a grain observed at 1 mm from the top of nugget zone.

junctions in their stable dihedral angle configuration. The Burke and Turnbull mechanism²⁶ of grain growth can operate in such a situation, which is based on the reduction in the grain boundary curvature formed between two triple junctions.

Although very fine grains are generally observed in the FSP microstructure, the top and middle of the nugget zone also possess some larger grains. These grains do not show any sign of abnormal grain growth; rather, they were formed by geometrical coalescence mechanism, proposed by Nielsen.²⁷ Geometrical coalescence occurs with the crystallographic texture

evolution, and the major criterion is same as the reduction in curvature at the grain boundary triple junctions. If grains of nearby orientations such as A and B in Fig. 5c come together and if the boundary that formed between them is of a lower angle boundary, then they will coalesce together and will form as a single grain. This might be possible in FSP where the deformation mode is simple shear and some of these deformation texture components are stable against dynamic recrystallization.²⁸

Possibility of static recrystallization (SRX) can be excluded from our consideration for the alloy owing to two possible reasons. PSN can also make the grain boundary shape more ragged than straight.²⁹ Abnormal grain growth was not observed in the nugget zone; rather, the coalescence of grains occurred due to the crystallographic texture development. This confirms that the time available during processing can be insufficient for SRX to take place.

Texture Evolution in the Nugget Zone

The deformation mode in FSP, though is simple shear, has the shear directions changing continuously during the process. Hence, it is possible that in different regions of the nugget zone, local textures can vary significantly. The bulk texture measured from the nugget zone can then be rather weak or it can be an entirely different component than any of the components that were observed locally. Dynamic recrystallization and the responsible

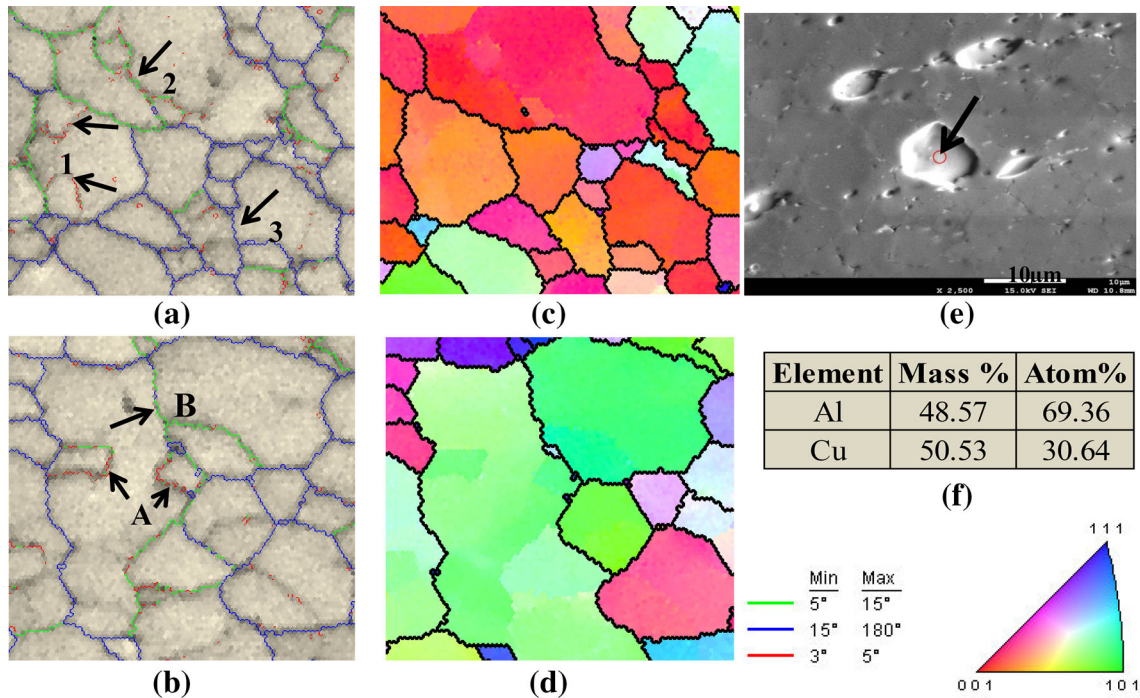


Fig. 5. Microstructural evolution in the nugget zone during FSP obtained from EBSD: (a and b) IQ map with grain boundaries super imposed. (c and d) IPF map corresponding to IQ maps in a and b. (e) Backscattered electron image showing a large precipitate particle observed at the top of nugget zone. (f) Composition of the same precipitate particle.

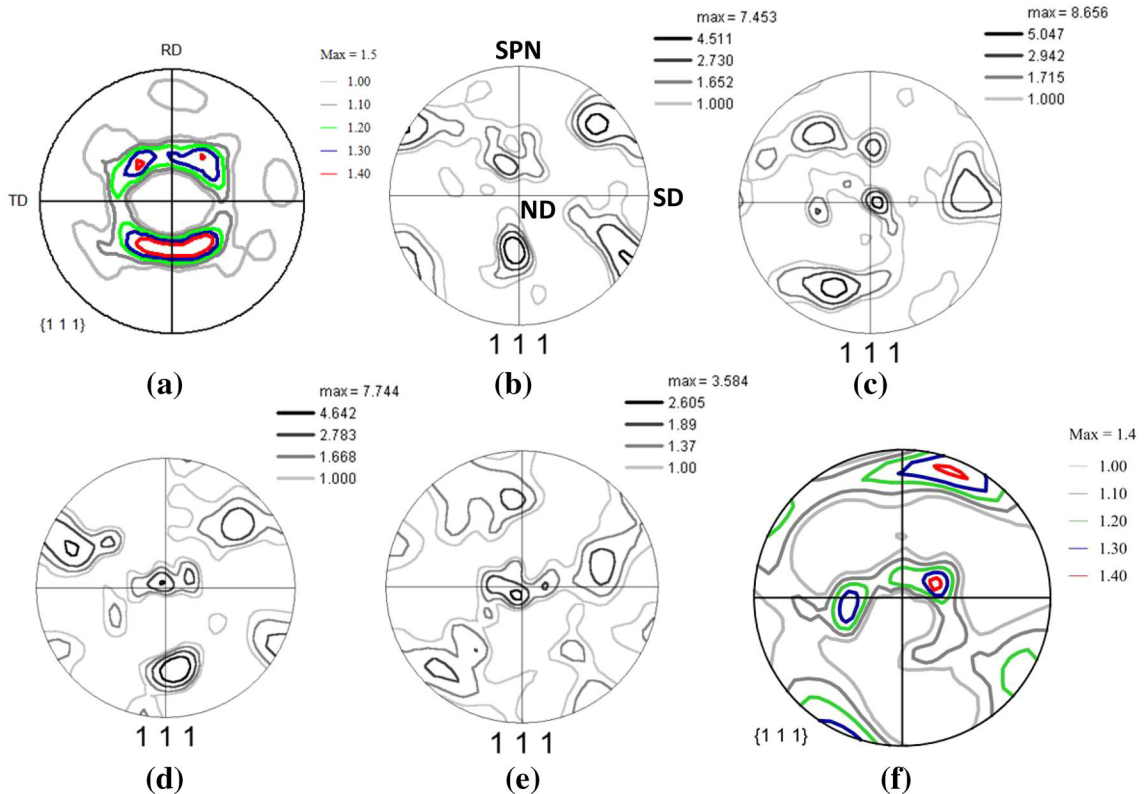


Fig. 6. (111) pole figure representation of (a) bulk texture of base metal, (b-e) microtexture in the nugget zone at (b) 200 μm from the top of nugget zone, (c) 1 mm from the top, (d) middle, and (e) 1.5 mm from the bottom. (f) Bulk texture for the optimum FSP sample. Reference frame for (c-f) are the same as (b) (ND = normal direction; SD = shear direction; SPN = shear plane normal).

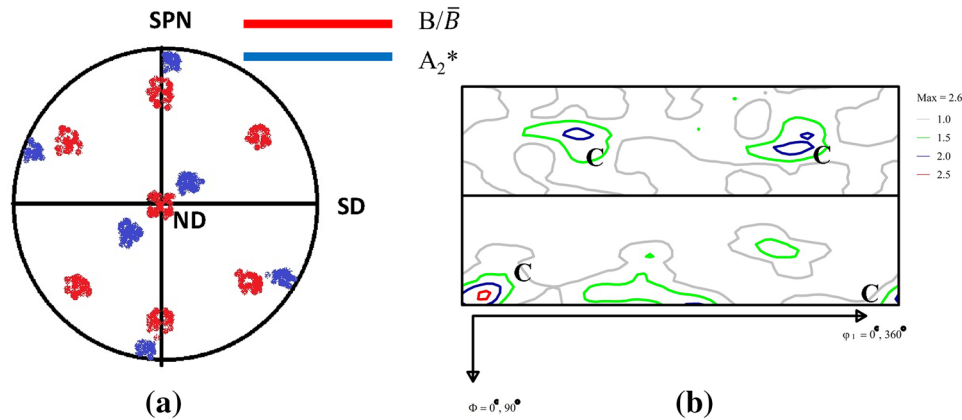


Fig. 7. (a) Microtexture observed in the middle and bottom of the nugget zone which is a combination of B/\bar{B} component and A_2^* . (b) Bulk texture in the nugget zone shown as φ_2 sections of 0° and 45° in ODF, C component is highlighted.

micromechanisms for the microstructure evolution during FSP can further complicate or increase the randomness of crystallographic texture present in processed materials. The bulk texture measured for the base metal is presented in Fig. 6a. The pole figures indicate the texture, which is typical of a recrystallized aluminum plate having mixed cube, rotated cube, and Goss texture components.

The microtextures present in the nugget zone across the thickness are shown in Fig. 6b–e. A dominant C component of shear texture is present at the extreme top of the nugget zone. This could be possible due to the higher shear strain at the extreme top of the nugget zone owing to the effect of tool shoulder. At 1 mm from the top of nugget zone, the microtexture has changed completely with the development of an entirely new set of texture components. The texture formation was completed at the middle of the nugget zone. The microtexture in the middle is a combination of B/\bar{B} and A_2^* components of shear texture, and this is shown schematically in Fig. 7. Such textures are reported in the worn bronze pins, during wear experiments done on a pin-on-disk tester.³⁰

At the bottom of the nugget zone due to the effect of a lesser strain and temperature, the intensity of texture has reduced significantly. The texture components in the bottom of the nugget zone are the same as that of the middle region. The bulk texture of the optimally processed FSP sample is shown Fig. 6f. It can be observed that the major texture component is A_2^* ; however, the overall texture is very weak. These results reinforce the previous statement that texture development during FSP of a heat-treatable alloy such as 2219 is a complex phenomenon. Even though the thermal conductivity of aluminum is reasonably high and could lead to faster heat removal during processing, the texture components vary across the thickness, even though all the measurements are made along same line. The B/\bar{B} components of shear texture are stable even at the high temperatures as observed in FSP.²⁸

The B/\bar{B} and C components have the same shear direction (110), which is also the most common slip direction in fcc materials. The presence of both these components in friction-stir processed materials could be due to the simple shear mode of deformation. The A_2^* component has the shear plane normal {111}, which is the most common slip plane in fcc materials. The most common recrystallization component of texture present in fcc material such as aluminum is the cube component and the nucleation of same occurs in bands known as cube bands ($\{001\}$ //ND rolling plane normal or shear plane normal in FSP). The nucleation of DRX can occur from such cube bands, and with the changes in direction due to the continuous stirring of the tool pin, C component can evolve more easily than other components.

CONCLUSION

A defect-free AA2219 material could be obtained using an optimized set of FSP parameters. Onion-ring formation in the nugget zone has been attributed to the crystallographic texture development in addition to age hardening response of the alloy. Microstructural evolution mechanism was a combination of shear deformation and dynamic recrystallization with the dominance of PSN. Normal grain growth was observed and the evolution of some large grains is attributed to geometrical coalescence which depends on the crystallographic texture development. Microtextural variation has been observed across the thickness of nugget zone. Shear texture components C and A_2^* are dominant in the nugget zone, and the evolution of both these occurred as a combined effect of simple shear deformation and DRX.

ACKNOWLEDGEMENTS

The authors would like to thank the Department of Science and Technology (DST), Ministry of Human Resources Development (MHRD), India, for financial

support and the Advanced Facility for Microscopy and Microanalysis (AFMM) at the Indian Institute of Science, Bangalore, India, for providing the characterization facilities. The authors are thankful to Vikram Sarabhai Space Centre (VSSC), Thiruvananthapuram, India for providing the aluminum alloy used in the work. N.N. is grateful to Government of Canada for Canadian Commonwealth Scholarship Program (CCSP).

REFERENCES

1. J.C. Williams and E.A. Starke, *Acta Mater.* 51, 5775 (2003).
2. R.Z. Valiev, R.K. Islamgaliev, and I.V. Alexandrov, *Prog. Mater. Sci.* 45, 103 (2000).
3. R.Z. Valiev, A.V. Korznikov, and R.R. Mulyukov, *Mater. Sci. Eng. A* 168, 141 (1993).
4. R.Z. Valiev, *Nat. Mater.* 3, 51 (2004).
5. S. Suwas, R.A. Massion, L.S. Tóth, J.J. Fundenberger, and B. Beausir, *Mater. Sci. Eng. A* 520, 134 (2009).
6. S. Suwas, R.A. Massion, L.S. Tóth, J.J. Fundenberger, and B. Beausir, *Metall. Mater. Trans. A* 37, 739 (2006).
7. S. Roy, B.R. Nataraj, S. Suwas, S. Kumar, and K. Chattopadhyay, *Mater. Des.* 36, 529 (2012).
8. S. Roy, D.S. Singh, S. Suwas, S. Kumar, and K. Chattopadhyay, *Mater. Sci. Eng. A* 528, 8469 (2011).
9. S. Biswas and S. Suwas, *Scripta Mater.* 66, 89 (2012).
10. N.P. Gurao, P. Kumar, A. Sarkar, H.G. Brokmeier, and S. Suwas, *J. Mater. Eng. Perform.* 22, 1004 (2013).
11. R.S. Mishra, M.W. Mahoney, S.X. McFadden, N.A. Mara, and A.K. Mukherjee, *Scripta Mater.* 42, 163 (1999).
12. Y. Iwahashi, J. Wang, Z. Horita, M. Nemoto, and T.G. Langdon, *Scripta Mater.* 35, 143 (1996).
13. G. Sakai, Z. Horita, and T.G. Langdon, *Mater. Sci. Eng. A* 393, 344 (2005).
14. K.S. Suresh, N. Kumar, R.S. Mishra, and S. Suwas, *Mater. Sci. Forum* 753, 247 (2013).
15. W. Xu, J. Liu, G. Luan, and C. Dong, *Mater. Des.* 30, 3460 (2009).
16. N. Nadammal, S.V. Kailas, and S. Suwas, *Mater. Des.* 65, 127 (2015).
17. R.W. Fonda, K.E. Knipling, and D.J. Rowenhorst, *JOM* 66, 149 (2014).
18. R. Nandan, T. Debroy, and H.K.D.H. Bhadeshia, *Prog. Mater. Sci.* 53, 980 (2008).
19. K. Kumar and S.V. Kailas, *Mater. Des.* 29, 791 (2008).
20. K.N. Krishnan, *Mater. Sci. Eng. A* 327, 246 (2002).
21. J.J. Jonas and L.S. Toth, *Scripta Metall. Mater.* 27, 1575 (1992).
22. M.A. Sutton, B. Yang, A.P. Reynolds, and R. Taylor, *Mater. Sci. Eng. A* 323, 160 (2002).
23. A. Rollett, F.J. Humphreys, G.S. Rohrer, and M. Hatherly, *Recrystallization and Related Annealing Phenomena* (New York: Elsevier, 2004).
24. K. Jata and S. Semiatin, *Scripta Mater.* 43, 743 (2000).
25. T.R. McNelley, S. Swaminathan, and J.Q. Su, *Scripta Mater.* 58, 349 (2008).
26. J.E. Burke and D. Turnbull, *Prog. Mater. Phys.* 3, 220 (1952).
27. J.P. Nielsen, *ASM Seminar Series* (Metals Park: American Society for Metals, 1966).
28. F. Montheillet, M. Cohen, and J.J. Jonas, *Acta Metall.* 32, 2077 (1984).
29. N. Hansen and B. Bay, *Acta Metall.* 29, 65 (1981).
30. W. Cai, J. Mabon, and P. Bellon, *Wear* 267, 485 (2009).